AUTOMATED CLASSIFICATION OF MAGNETIC RESONANCE BRAIN IMAGES USING BI-DIMENSIONAL EMPIRICAL MODE DECOMPOSITION

M.Tech. Thesis

By

OMKISHOR SAHU

DISCIPLINE OF ELECTRICAL ENGINEERING

INDIAN INSTITUTE OF TECHNOLOGY INDORE

JUNE 2015

AUTOMATED CLASSIFICATION OF MAGNETIC RESONANCE BRAIN IMAGES USING BI-DIMENSIONAL EMPIRICAL MODE DECOMPOSITION

A THESIS

Submitted in partial fulfillment of the
requirements for the award of the degree
of
Master of Technology
in
Electrical Engineering
with specialization in
Communication and Signal Processing

by

OMKISHOR SAHU
(1302102004)

DISCIPLINE OF ELECTRICAL ENGINEERING
INDIAN INSTITUTE OF TECHNOLOGY INDORE

JUNE 2015

INDIAN INSTITUTE OF TECHNOLOGY INDORE

CANDIDATE'S DECLARATION

I hereby certify that the work which is being presented in the thesis entitled "**AUTOMATED CLASSIFICATION OF MAGNETIC RESONANCE BRAIN IMAGES USING BI-DIMENSIONAL EMPIRICAL MODE DECOMPOSITION"** in the partial fulfillment of the requirements for the award of the degree of **MASTER OF TECHNOLOGY** with specialization in **COMMUNICATION AND SIGNAL PROCESSING** and submitted in the **DISCIPLINE OF ELECTRICAL ENGINEERING** at **Indian Institute of Technology Indore**, is an authentic record of my own work carried out during the time period from JULY 2014 to JUNE 2015 under the supervision of Dr. Ram Bilas Pachori, Associate Professor of Electrical Engineering, IIT Indore and Dr. Vivek Kanhangad, Assistant Professor of Electrical Engineering, IIT Indore .

The matter presented in this thesis has not been submitted by me for the award of any other degree of this or any other institute.

Signature of the student with date
(OMKISHOR SAHU)

This is to certify that the above statement made by the candidate is correct to the best of our knowledge.

Signature of the Supervisor
(DR. RAM BILAS PACHORI)

Signature of the Supervisor
(DR. VIVEK KANHANGAD)

OMKISHOR SAHU has successfully given his M.Tech. Oral Examination held on **29th June 2015**.

Signature of Supervisor of M.Tech. thesis
Date:

Convener, DPGC
Date:

Signature of PSPC Member
Date:

Signature of PSPC Member
Date:

ACKNOWLEDGEMENTS

First of all, i would like to express my sincere gratitude to my thesis supervisors **Dr. Ram Bilas Pachori** and **Dr. Vivek Kanhangad** for their constant support and guidance throughout this work.

I would also like to express my gratitude to my PSPC committee members Dr. Somnath Dey and Dr. Prabhat Kumar Upadhyay for their valuable suggestions.

I would also like to thank entire Department of Electrical Engineering for providing all the facilities and resources.

I would also like to thank all the faculty members of Electrical Engineering Department for teaching me during my course work which led to strong foundation for this work.

I would also like to thank Mr. Abhay Upadhyay, Mr. Rajeev Sharma and Mr. Vijay Anand, PhD Scholars, for their assistance at various stages of this work.

I am also thankful to all the members of Signal Analysis Lab for all their assistance.

I would also like to thank all the students of Electrical Engineering Research Lab for their help and guidance.

I would like to express my appreciation to my batch mates Sourabh, Jigar, Pradeep and Agnel for encouraging me through motivating and thoughtful discussions.

I am especially grateful to my family for their support and for believing in me.

Omkishor Sahu

M.Tech. (Communication and Signal Processing)

Discipline of Electrical Engineering

IIT Indore

Dedicated

to

My Family

Abstract

Automated classification of brain magnetic resonance (MR) images has been an extensively researched topic in biomedical image processing. In this work, we propose a new approach for classifying normal and abnormal brain MR images using bi-dimensional empirical mode decomposition (BEMD) and autoregressive (AR) model. In our approach, brain MR image is decomposed into bi-dimensional intrinsic mode functions (IMFs) using BEMD and AR coefficients from IMFs are used to form a feature vector. Finally, a binary classifier, least square support vector machine (LS-SVM), is employed to discriminate between normal and abnormal brain MR images. The proposed technique achieves 100% classification accuracy using second order AR model with linear and radial basis function (RBF) as kernels in LS-SVM clissifier. Experimental results also show that the performance of the proposed method is quite comparable with the existing results.

Contents

Abstract **i**

1 Introduction **1**

1.1 Magnetic resonance imaging 1

1.1.1 Image contrast 2

1.2 Brain abnormalities 2

1.3 Classification of MRIs 3

1.4 Related work 4

1.5 Organization 6

2 Proposed Methodology for Classification of Brain MRIs **7**

2.1 Empirical mode decomposition 7

2.2 Bidimensional empirical mode decomposition 10

2.2.1 Extrema detection 14

2.2.2 Image interpolation 15

2.3 Autoregressive model 15

2.3.1 1D autoregressive model 15

2.3.2 2D autoregressive model 16

2.4 Least square suppport vector machine 17

3 Results and Discussions **20**

4 Conclusions and Future Work **29**

4.1 Conclusions 29

4.2 Scope for future work 30

References **31**

List of Figures

1.1 Sample T1 weighted brain MR images: (a) Normal tissue, (b) Abnormal tissue. 3

1.2 Sample T2 weighted brain MR images: (a) Normal tissue, (b) Abnormal tissue. 4

2.1 Schematic diagram of the proposed approach for classifying brain MR images. 8

2.2 Sifting process to extract IMFs from the signal. 9

2.3 A sample 1D EEG signal and corresponding IMFs: (a) Signal, (b) First IMF, (c) Second IMF, (d) Third IMF, (e) Fourth IMF, (f) Fifth IMF, (g) Sixth IMF, (h) Seventh IMF, (i) Eighth IMF, (j) Ninth IMF, (k) Tenth IMF, (l) Eleventh IMF. 13

2.4 Feature space of SVM. 18

3.1 Sample brain MR images in the AANLIB database: (a) Normal, (b) Alzheimer's disease, (c) Glioma, (d) Herpes encephalitis, (e) Metastatic bronchogenic carcinoma, (f) Multiple sclerosis. 21

3.2 Sample normal brain MR image and corresponding IMFs: (a) Image, (b) First IMF, (c) Second IMF, (d) Third IMF, (e) Fourth IMF. 22

3.3 Sample abnormal brain MR image and corresponding IMFs: (a) Image, (b) First IMF, (c) Second IMF, (d) Third IMF, (e) Fourth IMF. 23

3.4 Plot of classification accuracy versus degree of polynomial kernel function in SVM. 27
3.5 Plot of classification accuracy versus sigma of RBF kernel function in SVM. 27

List of Tables

3.1 Distribution of abnormal brain MR images in database 20
3.2 Performance of the proposed approach for classification of brain MR images 28
3.3 Comparison of the proposed methodology with the existing methods studied on the same database 28

Chapter 1

Introduction

Computer aided diagnosis (CAD) [1] is a tool to help medical professionals in interpretation of medical images and medical decision making. Radiologists can use computer output as second opinion, and therefore CAD systems improve diagnosis accuracy. It combines image processing, artificial intelligence, computer vision, and statistical machine learning techniques. CAD systems have been used for classification of various types of images, for example images of brain, retina and mammograms etc [2].

1.1 Magnetic resonance imaging

Magnetic resonance imaging (MRI) is commonly used method for investigating brain abnormalities [3]. The MRI was developed based on observations in the experiments related to nuclear magnetic resonance (NMR). Therefore, the technique was called nuclear magnetic resonance imaging (NMRI). However, due to the negative connotation associated with the word nuclear the technique is generally referred to as MRI. MRI is a medical imaging technique used by radiologists to investigate internal structure of the body or any part of it [4]. MRI is preferred to computerized tomography (CT) as it does not use any ionizing radiation and both techniques provide same information [5]. Moreover, MRI is more sensitive to small tumors and provides better visualization making it preferred choice for detecting neurological cancers [6]. MRI is useful for cardiovascular [7], musculoskeletal [8], and oncological [9] imaging.

1.1.1 Image contrast

Contrast in the MR image is due to differences in the strength of the nuclear magnetic resonance (NMR) signal received from different locations in the brain [10]. Image contrast is dependent on relative density of excited nuclei and relaxation times (T1 and T2) of the nuclei after the pulse sequence.
Two contrast mechanisms [11] that are commonly used in brain MR imaging are discussed below:

1. **T1-weighted MRI**

   In T1-weighted MR imaging MR signal is measured after the magnetic field recovers. This is achieved by changing repetition time (TR). T1 weighted scans use short echo time (TE) and short repetition time (TR). For brain imaging, T1 weighted scans provide good contrast between gray matter and white matter [12, 13].

2. **T2-weighted MRI**

   In T2-weighted MR imaging MR signal is measured after the magnetic field decays. This is achieved by changing echo time (TE). T2 weighted scans use long TE and long TR. They are specially suited to detect edema [12, 13].

Figure 1.1 and 1.2 show samples of T1 weighted and T2 weighted MR images of brain from the database [14].

1.2 Brain abnormalities

Images of brain with some abnormalities are characterised by abrupt changes in image texture. For example, cancer in brain magnetic resonance image is characterised by large cells with high contrast [15], thus making it feasible to differentiate them from normal brain magnetic resonance images. Alzheimers disease [16] is the common cause of age-related dementia. Multiple sclerosis [17] is a neurological disorder that results in various dysfunctions. Other abnormalities related to the brain include glioma, herpes encephalitis and metastatic bronchogenic carcinoma etc [18–20]. Images of brain having above mentioned diseases are characterized by large cells and high contrast. Many methods have been proposed in the literature to identify brain MR images having aforementioned abnormalities. Abnormal images may have one or multiple abnormalities.

1.3 Classification of MRIs

Generally, the classification of medical images is performed using a two step procedure. In the first step, discriminating information or features are extracted from medical images.

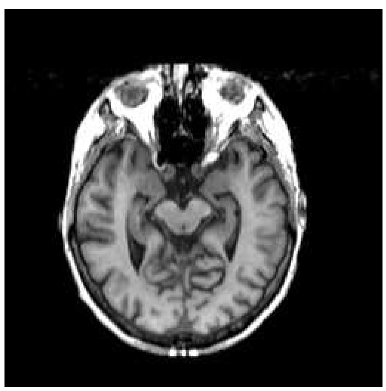

(a)

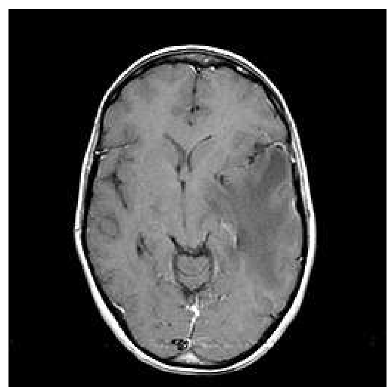

(b)

Figure 1.1: Sample T1 weighted brain MR images: (a) Normal tissue, (b) Abnormal tissue.

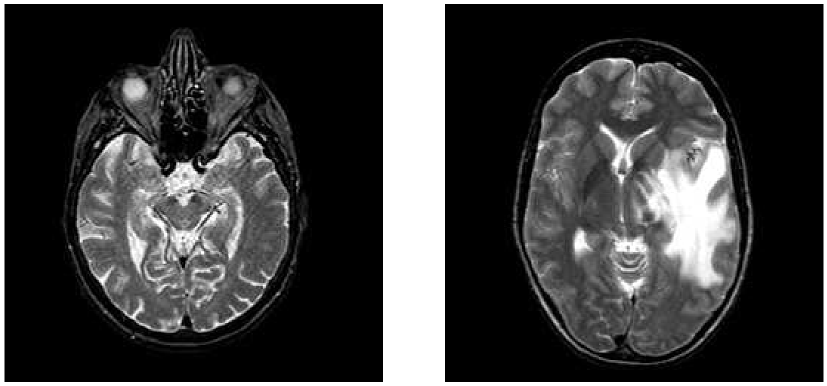

(a) (b)

Figure 1.2: Sample T2 weighted brain MR images: (a) Normal tissue, (b) Abnormal tissue.

In the second step, a classifier utilizes the extracted information to form a decision on the category of the input image. Classification approaches are of two types, supervised and unsupervised. Supervised methods include support vector machines (SVM) [18], artificial neural network (ANN) [20] and K-nearest neighbor (KNN) [19]. Unsupervised classification techniques includes self-organization map (SOM) [18] and fuzzy c-means [21]. Supervised methods are more common than unsupervised methods because they usally provide better accuracies [22].

1.4 Related work

In recent years, extensive research has been done in the area of automated classification of MR images of normal and abnormal brain. Two-dimensional discrete wavelet transform (2D-DWT) based approaches have been extensively explored for classification of brain MR images. Specifically, the approaches presented in [18,23] explored approximation coefficients at level 2 and level 3 for discrimination, while the work in [24] presented an approach based on two-dimensional discrete wavelet transform (2D-DWT) for feature extraction, principal component analysis (PCA) for feature space reduction and back propagation neural network for classification of MR images. In another related work [25], generalized autoregressive conditional heteroscedasticity (GARCH) was employed to model wavelet coefficients of detail sub-bands to obtain feature vector for classification of MR images.

Authors in [26] used the coefficients of the approximation sub-band of two-level 2D-DWT of brain MRI as features, and self-organization map (SOM) based neural network and SVM for classification. Maitra et al. [27] applied slantlet transform on intensity histogram of the image and employed back propagation neural network (BPNN) for classification of MR images. Authors in [19] proposed a hybrid method for brain MR image classification using wavelet transform and PCA. Scaled conjugate gradient was used for optimal weight setting in BPNN for classification of MR images. Saritha et al. [28] used wavelet entropy based spider web plots for feature extraction and probabilistic neural network for classification to achieve maximum classification accuracy. In [29], authors proposed a three-stage approach for brain MR image classification using features extracted from LH and HL sub-bands of two level 2D-DWT with ensemble classifier. Subsequently, authors in [20] employed 2D-DWT followed by Gabor filter banks on HH sub-band of 2D-DWT for feature extraction and SVM for classification of MR images. Lahmiri et al. [30] employed 1D-EMD to generate intrinsic mode functions (IMFs) from brain MR images. In this approach conversion of brain MR image to one dimensional signal is done by concatenating successive rows of the image from left to right and top to down. Statistical features were extracted from the IMFs and an entropy based selection process was employed to identify the most informative features from each IMF followed by SVM for classification. A detailed survey of CAD of human brain tumor using MR images is presented in [31]. Authors in [31] also proposed a new approach employing the feedback pulse coded neural network for image segmentation followed by DWT and PCA for feature extraction and forward BPNN for classification of MR images.

In the presented work, we have proposed an approach for classification of normal and abnormal brain MR images. To the best of our knowledge, this is the first time that bi-dimensional empirical mode decomposition (BEMD) is applied for classification of brain

MR images. Experimental results show that the proposed approach has outperformed existing approaches in terms of classification accuracy.

1.5 Organization

The rest of the thesis is organized as follows: A detailed description of the proposed methodology is presented in Chapter 2, which includes brief review of AR model, EMD, BEMD and SVM. Chapter 3 presents experimental results and discussion, followed by concluding remarks in Chapter 4.

Chapter 2

Proposed Methodology for Classification of Brain MRIs

The classification of brain MR images is carried out in a three step process. Firstly, bi-dimensional empirical mode decomposition (BEMD) is used to decompose the image into the intrinsic mode functions (IMFs). This is followed by modelling of individual IMFs using autoregressive (AR) model to generate feature vectors in the form of AR coefficients. Finally, based on the extracted features least square support vector machine (LS-SVM) makes a decision as to whether the input brain MR image is of normal or abnormal human brain. The schematic diagram of the proposed methodology is presented in Figure 2.1.

2.1 Empirical mode decomposition

Empirical mode decomposition (EMD) [32] is a multi-resolution decomposition technique. EMD represents a nonstationary signal as a sum of of zero-mean amplitude modulation frequency modulation (AM-FM) components [33]. The decomposition process is adaptive and signal dependent. The decomposition does not require any condition on the signal about linearity and singularity. It is suited for the analysis of 1D nonlinear and non-stationary signals. EMD decomposes a 1D signal into a set of band-limited

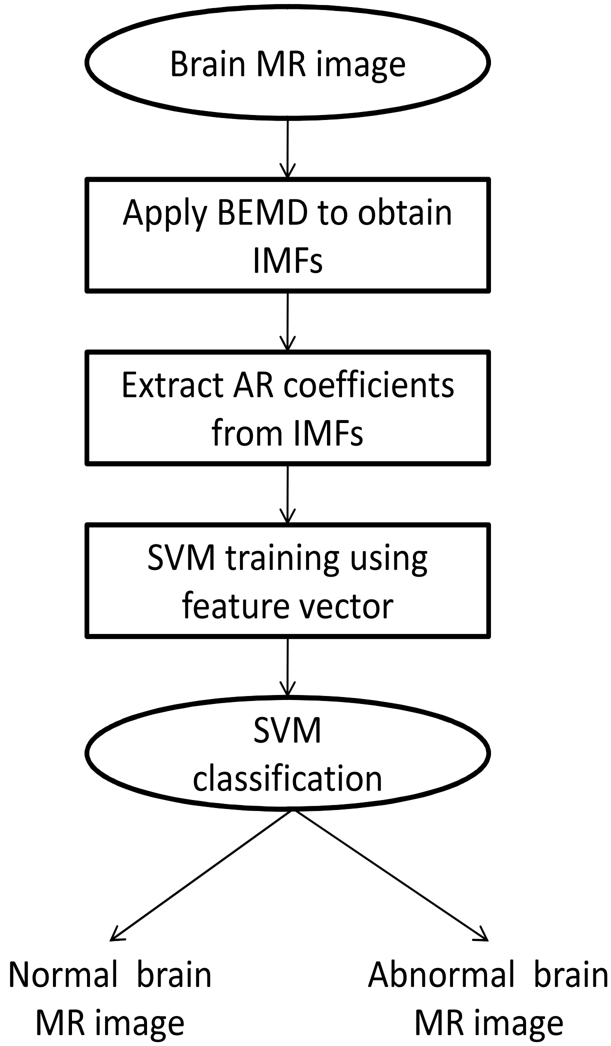

Figure 2.1: Schematic diagram of the proposed approach for classifying brain MR images.

signals called intrinsic mode functions (IMFs).The procedure used to extract IMFs from the signal is termed as sifting.

The decomposition is based on the following assumptions [32]:

1. The signal should have at least one maxima and one minima).

2. The time scale depends on the time interval between the extrema points.

3. If the data does not have any extrema and contains only inflection points, then it can be differentiated multiple times to obtain the extrema. The integration operation can be applied after the processing of these components.

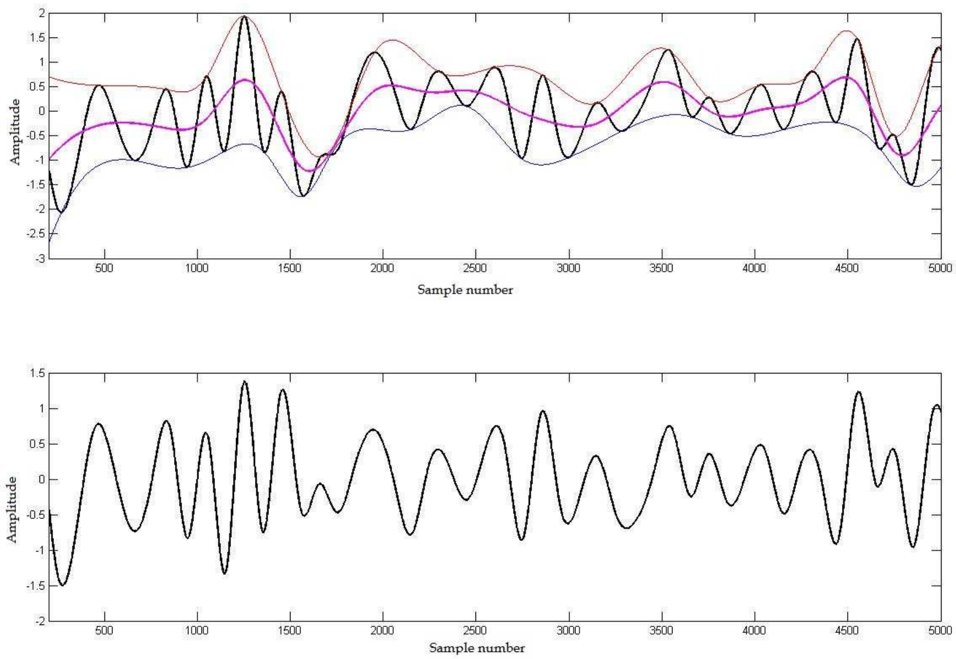

Figure 2.2: Sifting process to extract IMFs from the signal.

IMFs obtained from the 1D signal using sifting process satisfy two basic conditions [32]:

1. The total number of maxima and minima and the total number of zero-crossings should be equal or different by one.

2. At any sample instant, the average value of the envelopes specified by the local maxima and the local minima should be equal to zero.

The first condition is identical to the narrow-band requirement for a stationary Gaussian process. The second condition is required so as to avoid unwanted fluctuations induced by asymmetric wave forms for instantaneous frequency.

Sifting process is depicted in Figure 2.2. For signal $x(t)$, sifting process can be summarized as follows [32]:

1. Let $g(t) = x(t)$.

2. obtain the extrima from $g(t)$.

3. find out upper envelope $e_u(t)$ and lower envelope $e_l(t)$ by connecting maxima and minima respectively.

4. Compute the mean envelope $e_m(t)$ by averaging these two envelopes as

$$e_m(t) = \frac{e_u(t) + e_l(t)}{2}$$

5. Subtract $e_m(t)$ from the signal $g(t)$ as $g(t) = g(t) - e_m(t)$.

6. Determine whether $g(t)$ is a valid IMF or not, by applying conditions of IMF.

7. If $g(t)$ is not a valid IMF, repeat steps 2 to 6 until a valid IMF $g(t)$ is obtained.

Once a valid IMF is obtained, assign $D_1(t) = g(t)$. Obtain $r(t)$ by applying subtraction operation as $r(t) = x(t) - D_1(t)$. Replace $x(t)$ by $r(t)$ i.e. $x(t) = r(t)$. To generate the next IMF, repeat steps 2 to 7 by considering $g(t) = r(t)$. The signal $x(t)$ can be represented as follows [32]:

$$x(t) = \sum_{i=1}^{M} D_i(t) + r(t) \tag{2.1}$$

where M represents total number of the IMFs present in the signal and $r(t)$ is the residual component of the signal.

Figure 2.3 shows a sample 1D EEG signal and corresponding IMFs extracted from it.

EMD has numerous applications in various areas such as electroencephalogram (EEG) signal analysis [34–40], gear fault diagnosis [41], analysis of center of pressure (COP) signals [42] and speech signal analysis [43].

2.2 Bidimensional empirical mode decomposition

Bidimensional empirical mode decomposition (BEMD) is used to obtain 2D IMFs using the sifting method. A 2D IMF can be considered as a zero-mean 2D AM-FM component [44].

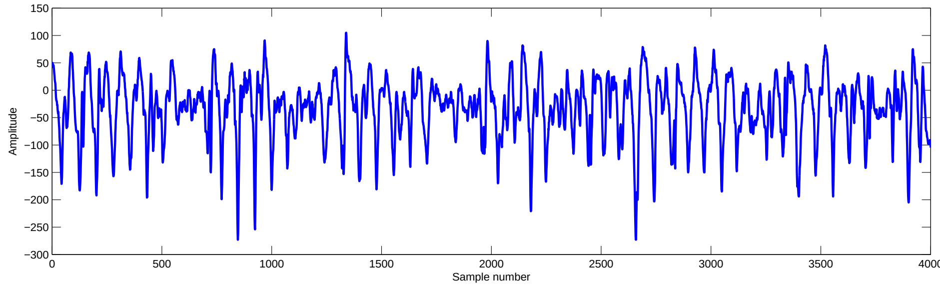

Amplitude
Sample number

(a)

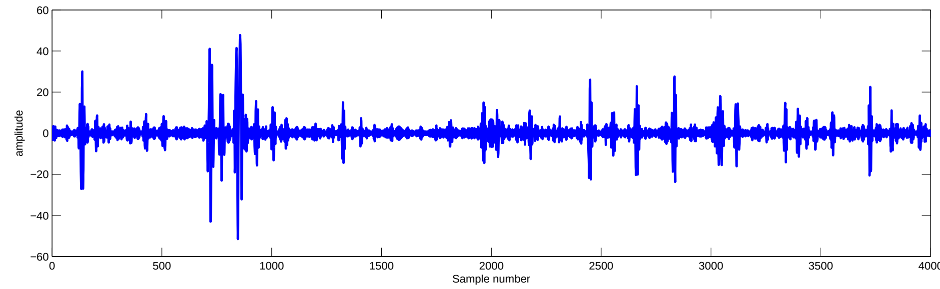

amplitude
Sample number

(b)

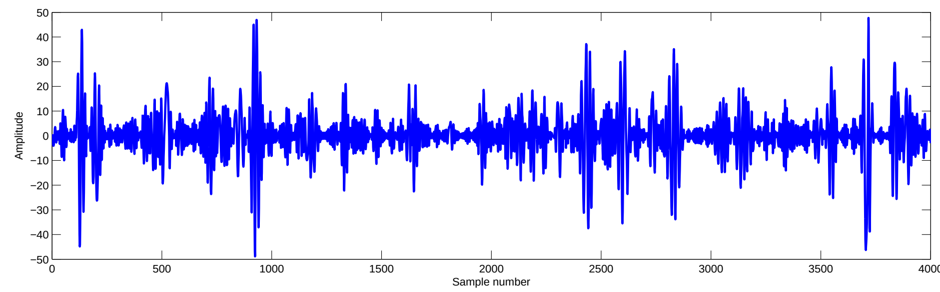

Amplitude
Sample number

(c)

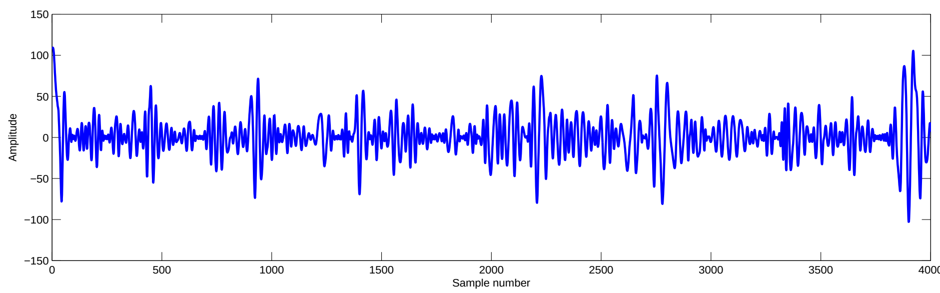

Amplitude
Sample number

(d)

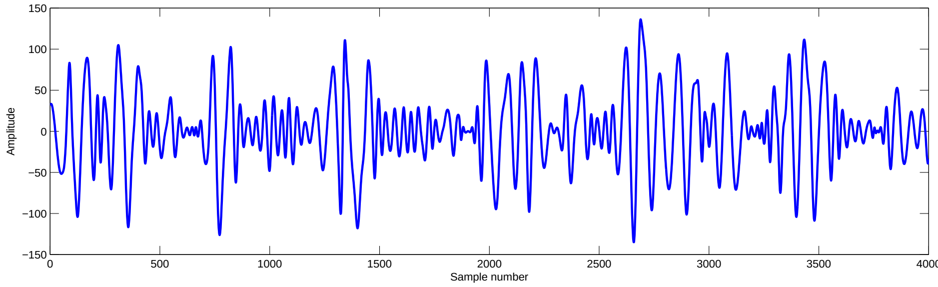

Amplitude
Sample number

(e)

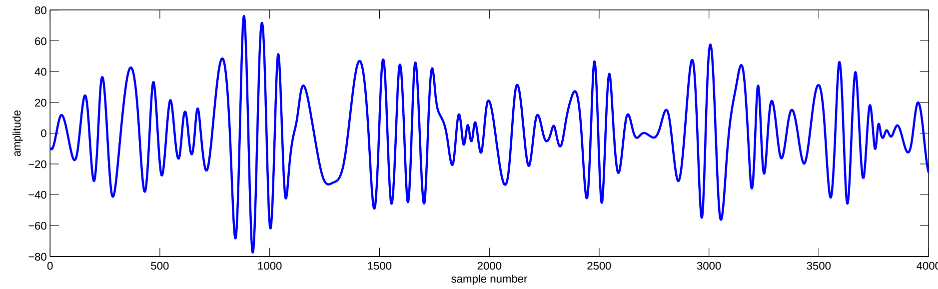

amplitude
sample number

(f)

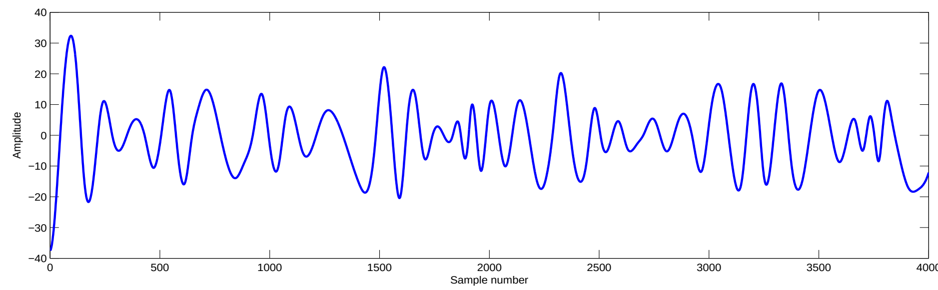

Amplitude
Sample number

(g)

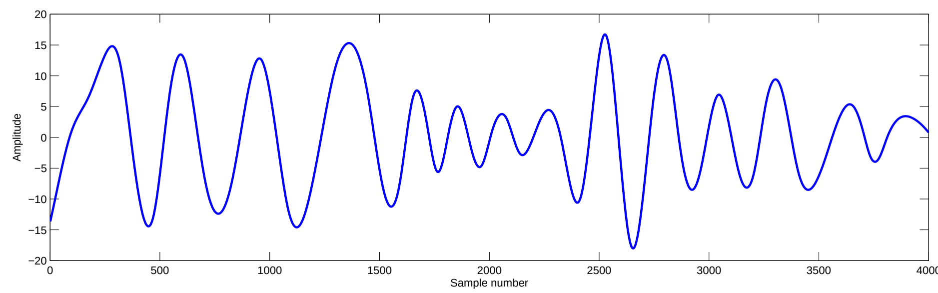

Amplitude
Sample number

(h)

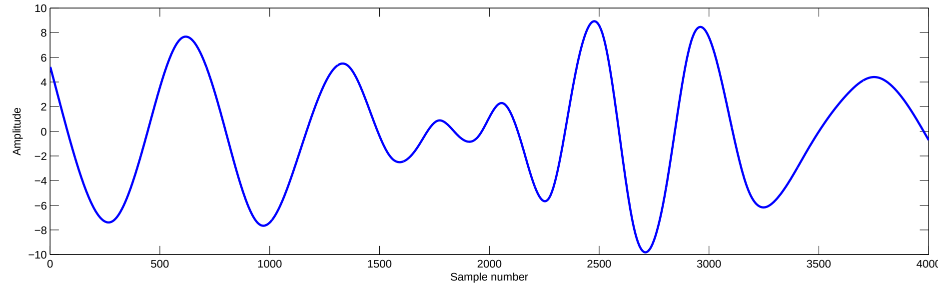

(i)

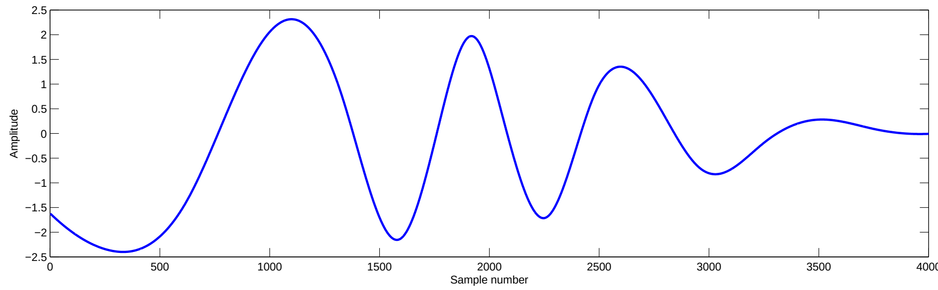

(j)

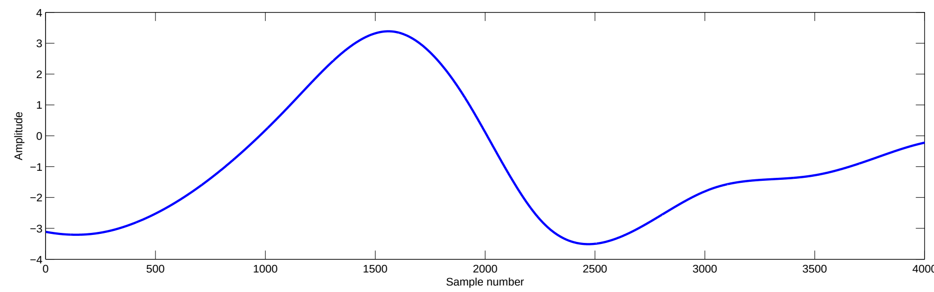

(k)

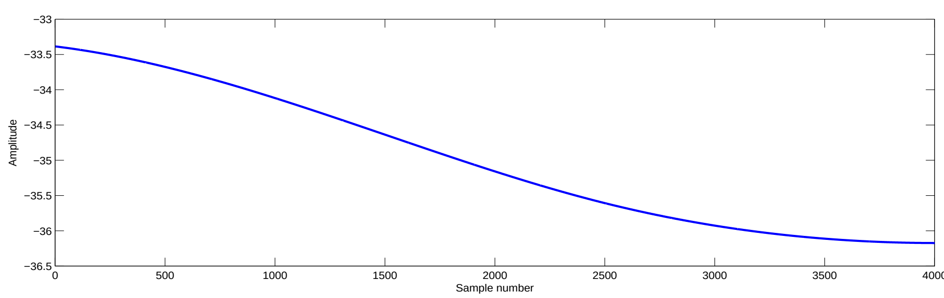

(l)

Figure 2.3: A sample 1D EEG signal and corresponding IMFs: (a) Signal, (b) First IMF, (c) Second IMF, (d) Third IMF, (e) Fourth IMF, (f) Fifth IMF, (g) Sixth IMF, (h) Seventh IMF, (i) Eighth IMF, (j) Ninth IMF, (k) Tenth IMF, (l) Eleventh IMF.

BEMD has applications in many areas such as texture analysis [45, 46], image denoising [47], image watermarking [48], iris recognition [49], image fusion [50], image feature extraction [51], image classification [52], texture classification and segmentation [53], etc. For BEMD technique MATLAB codes are available at MATLAB central file exchange [54].

Bidimensional sifting process [44, 55] can be summarized as:

1. Locate the extrema points of the image I based on morphological reconstruction using geodesic operators [56].

2. Interpolate the surface between all the maxima and all the minima with RBF to build the 2D envelope X_{max} and X_{min}, respectively [57].

3. Determine the mean envelope X_m using average of the two envelopes as follows:

$$X_m = \frac{X_{max} + X_{min}}{2}$$

4. subtract out the mean from the image to get $h_1 = I - X_m$.

5. Repeat the above mentioned process till h_1 satisfy conditions of an IMF.

2.2.1 Extrema detection

To detect the image extrema geodesic operators based morphological reconstruction has been used. To obtain grayscale reconstruction $Ir_I(J)$ of I from J grayscale geodesic dilations ∂_1^n of J under I is iterated until a stability is reached, i.e. $Ir_I = \bigvee_{n \geq 1} \partial_1^n(J)$. To detect the maxima following procedure has been used [58]:

1. Subtract one gray level from every pixel of original image I to construct J, i.e. $J = I - 1$

2. Perform reconstruction Ir of J by I by geodesic dilation

3. Subtract Ir from I to obtain the indicator function of maxima of I.

Similarly, to detect the minima following procedure has been used [58]:

1. Subtract one gray level from every pixel of original image I to construct J, i.e. $J = I - 1$

2. Perform reconstruction Ir of J by I by geodesic erosion.

3. Subtract Ir from I to obtain the indicator function of minima of I.

2.2.2 Image interpolation

RBF function has been used for interpolation. A RBF function is defined as [57]:

$$s(x) = p_m(x) + \sum_{i=1}^{N} \lambda_i \Phi(\|x - x_i\|), x \in R^d, \lambda_i \in R \tag{2.2}$$

where s is the radial basis function, p_m represents low degree polynomial, typically linear or quadratic, a member of m^{th} degree polynomials in d variables, $\|.\|$ denotes the Euclidian norm, the λ_i's are the RBF coefficients, Φ is a real valued function called the basic function, x_i's are the RBF centres.

2.3 Autoregressive model

Autoregressive model (AR) is used in signal processing and statistics for representing signals based on parametric approach. The AR model specifies that output variable of a process is linearly dependent on it's previous output's. AR model is a special case of autoregressive moving average (ARMA) model.

2.3.1 1D autoregressive model

1D AR model of order p is defined as [59]:

$$X(t) = \sum_{i=1}^{p} a_i X(t-i) + w(t) \tag{2.3}$$

where, a_i are known as AR parameters and w represents white noise. From 2.3 AR model can be considered as output of all pole filter with white noise as input. Yule-Walker equations can be used to determine the AR model parameters.

2.3.2 2D autoregressive model

A 2D AR model for image analysis is explained in [60]. In our study, 2D AR model is employed on 2D IMFs of the brain MR images. In order to analyze 2D IMFs with 2D AR model, it is considered as a 2D random field $x[p,q], (p,q) \in Z^2$. For the $N_1 \times N_2$ image $I = \{x[p,q] : 0 \leq p \leq N_1 - 1, 0 \leq q \leq N_2 - 1\}$, 2D AR (r_1, r_2) model is defined by the following difference equation [60]:

$$x[p,q] + \sum_{i=0}^{r_1} \sum_{j=0}^{r_2} a_{ij} x[p-i, q-j] = w[p,q] \tag{2.4}$$

where $w[p,q]$ is a stationary white noise field with variance σ^2, r_1 and r_2 represent order of the AR model and the coefficients a_{ij} are the parameters of the 2D AR model.
In (2.4), the image $x[p,q]$ can be interpreted as the output of the linear time-invariant (LTI) causal system with transfer function $H(z_1, z_2)$ and a white noise as an input. The transfer function is given as [60]:

$$H(z_1, z_2) = \frac{1}{A(z_1, z_2)} = \frac{1}{\sum_{i=0}^{r_1} \sum_{j=0}^{r_2} a_{ij} z_1^{-i} z_2^{-j}} \tag{2.5}$$

with $a_{00} = 1$. Assuming that the noise sequence $w[p,q]$ are known, the parameters in the AR model (2.4) can be determined by the least-squares (LS) method as follow [60]:

$$x[p,q] + \phi^T[p,q]\theta = w[p,q] \tag{2.6}$$

where

$$\phi^T[p,q] = [x[p,q-1], \cdots, x[p-r_1, q-r_2]] \tag{2.7}$$

and

$$\theta = [a_{01}, \cdots, a_{r_1 r_2}]^T \tag{2.8}$$

The matrix form of (2.6) for $p = L+1, \cdots, N_1 - 1$, and $q = M+1, \cdots, N_2 - 1$, for arbitrary $L > r_1$, and $M > r_2$, provides [60]:

$$X + \Phi\theta = W \tag{2.9}$$

where

$$X = [x[L{+}1, M{+}1], \cdots, x[N_1{-}1, N_2{-}1]]^T, W = [w[L{+}1, M{+}1], \cdots, w[N_1{-}1, N_2{-}1]]^T$$

and Φ is given as [60]:

$$\Phi = \begin{pmatrix} x[L+1,1] & \cdots & x[L+1-r_1, M+1-r_2] \\ x[L+2,1] & \cdots & x[L+2-r_1, M+1-r_2] \\ \vdots & \ddots & \vdots \\ x[N_1-1, N_2-1] & \cdots & x[N_1-1-r_1, N_2-1-r_2] \end{pmatrix}$$

Assuming that Φ is known, a least-squares estimate of the parameter vector θ in (2.9) can be obtained as [60]:

$$\hat{\theta} = -(\Phi^T\Phi)^{-1}\Phi^T X \tag{2.10}$$

AR model has been employed for many applications such as shape classification [61], electroencephalogram (EEG) and electrocardiogram (ECG) signal classification [62,63], image texture analysis [64], etc.

2.4 Least square suppport vector machine

SVM was introduced in [65]. It is based on statistical learning theory. To classify the data, SVM constructs optimal separating hyperplane which maximizes the separation between the two nearest data points which belongs to two different classes.

Figure 2.4 demonstrates basic concept of SVM. As shown in figure there are two different sets of data represented by o and $\diamond$. Hyperplane P_1 is not a good solution because it does not separate two datasets completely. Between two possible solutions P_2 and P_3, hyperplane P_3 is an optimal solution because it provides maximum margin between two datasets.

Consider N number of data points $\{x_i, y_i\}_{i=1}^{N}$, where $x_i \,\epsilon\, R$ is input and $y_i \,\epsilon\, \{+1, -1\}$ is class label.

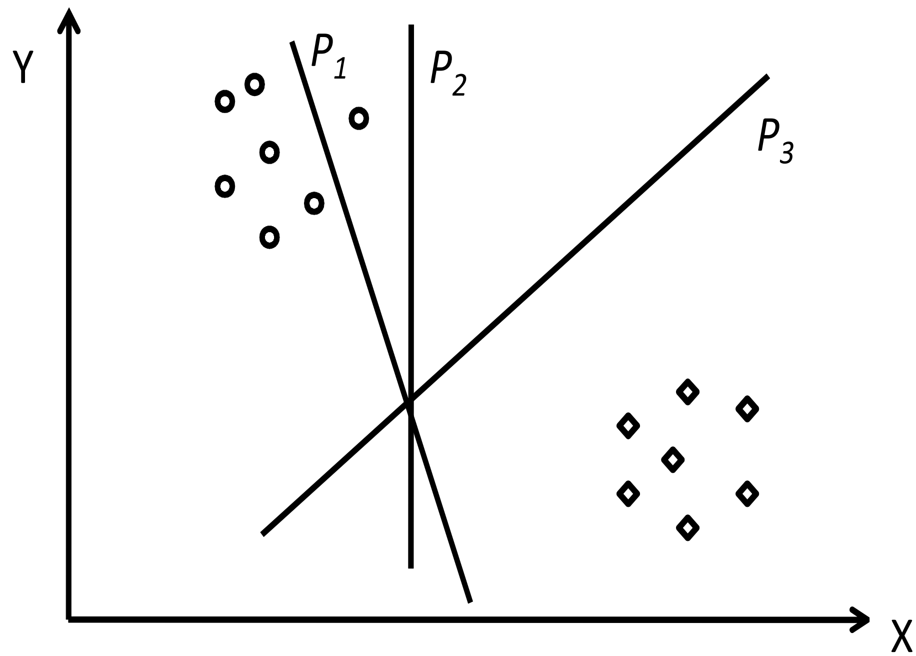

Figure 2.4: Feature space of SVM.

For two-class classification problem, separation hyperplane is given as [66]:

$$f(x) = \text{sign}[\Omega^T g(x) + \beta] \tag{2.11}$$

where Ω is d-dimensional weight vector and *g(x)* is a mapping function that maps x into the d-dimensional space and β is a bias. The least square version of SVM, which is known as least-square SVM (LS-SVM) was introduced in [67]. The classification problem using LS-SVM can be formulated as [67]:

$$\min\ J(\Omega, \beta, \varepsilon) = \frac{1}{2}\,\Omega^T\Omega\ +\ \frac{\gamma}{2}\sum_{i=1}^{N}\varepsilon_i^2 \tag{2.12}$$

subject to the following equality constraint,

$$y_i[\Omega^T g(x_i) + \beta] = 1 - \varepsilon_i, i = 1, 2, \ldots, N \tag{2.13}$$

where $\varepsilon = (\varepsilon_1, \varepsilon_2, \cdots, \varepsilon_N)^T$.

The Lagrangian multiplier α_i for (2.12) can be defined as [67]:

$$L(\Omega, \beta, \varepsilon; \alpha) = J(\Omega, \beta, \varepsilon) - \sum_{i=1}^{N} \alpha_i \{y_i[\Omega^T g(x_i) + \beta] - 1 + \varepsilon_i\} \tag{2.14}$$

On solving (2.14) by considering the optimal conditions, LS-SVM classifier is obtained as [67]:

$$f(x) = \text{sign}\left(\sum_{i=1}^{N} \alpha_i y_i K(x, x_i) + \beta\right) \tag{2.15}$$

where $K(x, x_i)$ is kernel function. In the presented work, different kernel functions have been used which are defined as follows [66]:

1. Linear kernel function:

$$K(x, x_i) = x.x_i \tag{2.16}$$

2. Polynomial kernel function:

$$K(x, x_i) = (x.x_i + 1)^d \tag{2.17}$$

   where d is the degree of the polynomial.

3. Radial basis function (RBF) kernel:

$$K(x, x_i) = e^{\frac{-\|x - x_i\|^2}{2\sigma^2}} \tag{2.18}$$

   where σ controls the width of RBF function.

LS-SVM has been widely used for classification of EEG signals [68,69], ECG signals [70], electromyogram (EMG) signals [71], MR images [72], etc.

Chapter 3

Results and Discussions

Experimental evaluation of the proposed method was performed on a publicly available AANLIB database of Harvard medical school [14]. Figure 3.1 presents a set of brain MR images from the database. For our experiments, a total of 88 axial, T2-weighted brain MR images are used, out of which 25 images correspond to normal human brain and the remaining 63 images correspond to human brain affected by diseases such as herpes encephalitis, alzheimer's, glioma, metastatic bronchogenic carcinoma and multiple sclerosis. Number of images corresponding to each of these diseases is presented in Table 3.1.

Table 3.1: Distribution of abnormal brain MR images in database

Disease	Number of images
Alzheimer's	10
Glioma	12
Herpes encephalitis	16
Metastatic bronchogenic carcinoma	11
Multiple sclerosis	14

In our experiments, BEMD is applied on each of the brain MR images to extract 2D IMFs. Figures 3.2 and 3.3 show a sample brain MR image and corresponding IMFs

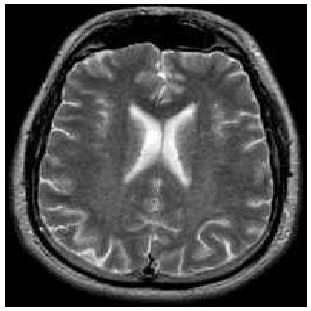 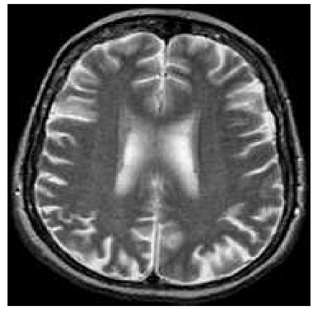

(a) (b)

 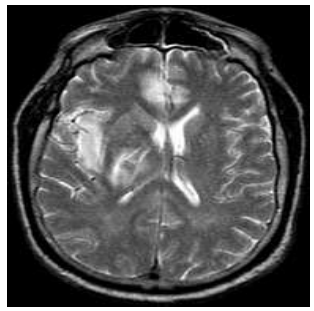

(c) (d)

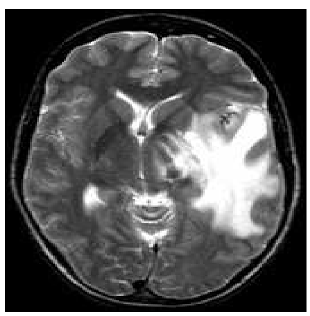 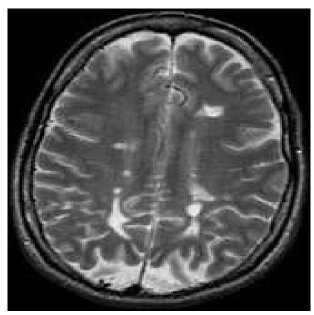

(e) (f)

Figure 3.1: Sample brain MR images in the AANLIB database: (a) Normal, (b) Alzheimer's disease, (c) Glioma, (d) Herpes encephalitis, (e) Metastatic bronchogenic carcinoma, (f) Multiple sclerosis.

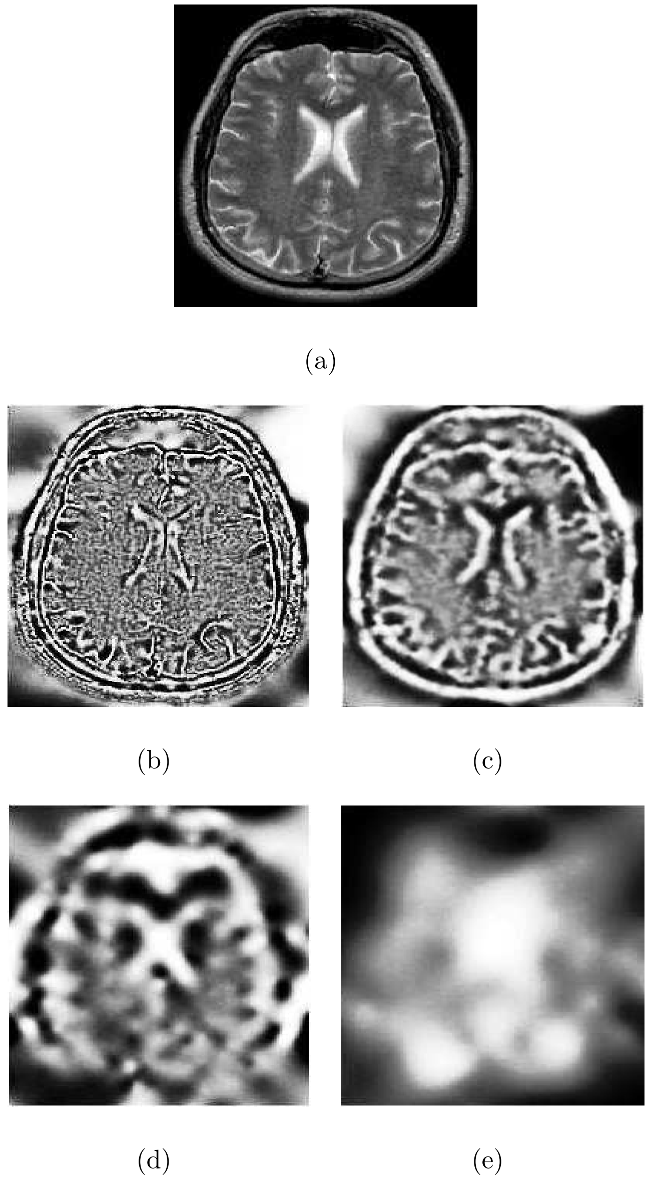

Figure 3.2: Sample normal brain MR image and corresponding IMFs: (a) Image, (b) First IMF, (c) Second IMF, (d) Third IMF, (e) Fourth IMF.

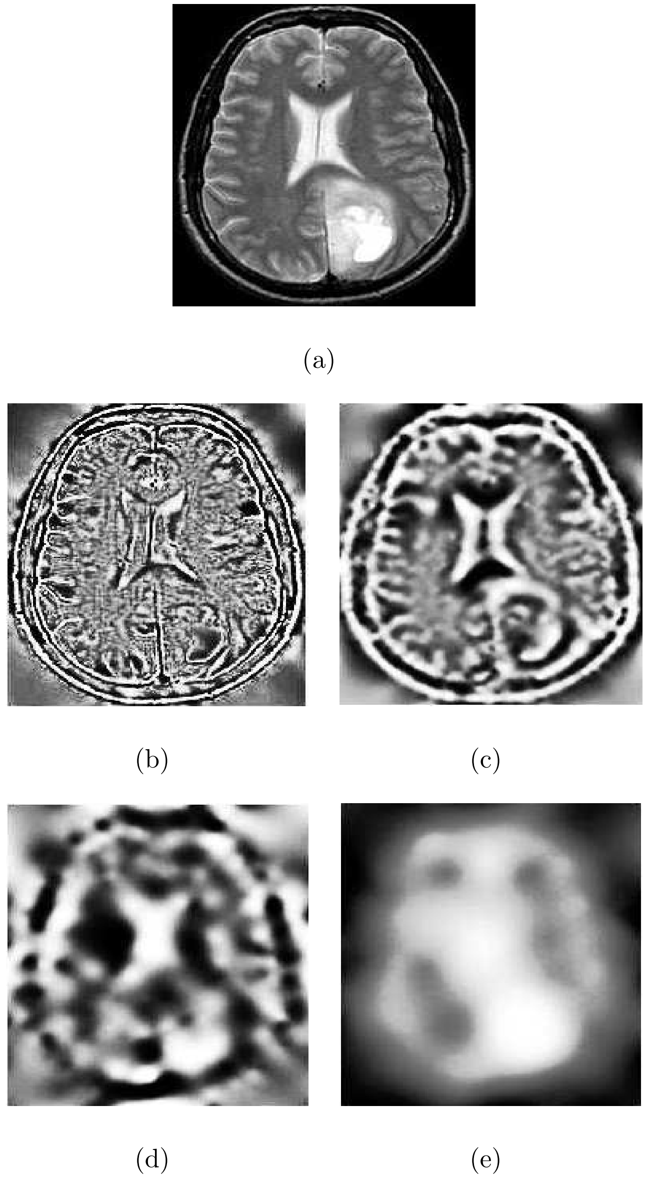

Figure 3.3: Sample abnormal brain MR image and corresponding IMFs: (a) Image, (b) First IMF, (c) Second IMF, (d) Third IMF, (e) Fourth IMF.

for normal and abnormal category, respectively.

As can be observed from Figures 3.2 and 3.3, the visual information contained in 2D IMFs decreases as the mode of 2D IMFs is increased. Therefore, in our experiments, only the first four 2D IMFs are used for further processing.

In our approach, each of the 2D IMF is modeled using a 2D AR model. In this way, we obtained AR coefficients for each of the IMFs, which are concatenated to form the feature vectors. Finally, LS-SVM is employed for classification of brain MR images. A set of experiments have been performed to investigate the performance of our approach with different orders of the AR model and different kernel functions of SVM. Specifically, the performance of the proposed methodology is evaluated with linear, polynomial and RBF kernel functions in SVM for 1st, 2nd and 3rd order AR models. In addition, in order to study the effect of kernel parameters on the classification accuracy, we performed experiments by varying the degree of the polynomial kernel from 2 to 4 in steps of 1. Similarly, the sigma (σ) value of RBF kernel function was varied from 0.1 to 10 in steps of 0.1. Specifically, we have performed 10-fold cross validation experiments.

Performance of the proposed method was evaluated using performance measures such as accuracy, sensitivity and specificity. Suppose TP and TN represent the number of correctly classified positive and negative samples and FP and FN represent the number of falsely classified negative and positive samples respectively. The performance measures are defined as follows [73]:

1. Accuracy (ACC): It is defined as the fraction of correctly classified positives and negative samples out of the total number of test samples and it is given as:

$$ACC = \frac{TP + TN}{TP + TN + FP + FN} \times 100 \tag{3.1}$$

2. Sensitivity (SEN): It is defined as the ratio of numbers of correctly classified positive samples to the total number of positive test samples and it is given as:

$$SEN = \frac{TP}{TP + FN} \times 100 \tag{3.2}$$

3. Specificity (SPF): It is defined as ratio of number of correctly classified negative samples to the total number of negative test samples and it is given as:

$$SPF = \frac{TN}{TN + FP} \times 100 \tag{3.3}$$

A plot of classification accuracy vs degree of polynomial kernel function in SVM is shown in Figure 3.4, from which it can be observed that 1st order AR model provides the least classification accuracy consistently for for 2nd, 3rd and 4th degree polynomial kernel function. On the other hand, 2nd and 3rd order AR models achieve maximum accuracy for 2nd degree of polynomial kernel function in SVM.

Figure 3.5 presents a plot of classification accuracy vs sigma values for RBF kernel function in SVM obtained by varying sigma values from 0.1 to 10. It can be observed from the Figure 3.5 that accuracy of 1st order AR model varies significantly for different values of sigma and the accuracy decreases as sigma value is increased. 1st order AR model achieves accuracy less than 97% for all values of sigma, whereas 2nd order AR model achieves 100% accuracy for sigma values greater than 8 and 3rd order AR model achieves 100% accuracy for sigma values greater than 6.5. Thus, it can be concluded that 3rd order AR model achieves the maximum accuracy for the least value of sigma.

The results of our experiments are summarized in the Table 3.2. From the results, it is observed that the 2nd order linear and RBF kernel function achieves 100% accuracy, sensitivity and specificity. Polynomial function achieves a maximum classification accuracy of 99% for 2nd degree polynomial and 2nd order AR model. Also it can be noticed that in the case of 2nd order AR model, Linear kernel function provides better accuracy as compared to polynomial (Non-linear) kernel function. This may be due to overfitting, which occurs when model is excessively complex and size of training dataset is too small in comparison to model complexity. Overfitting can be considered as a situation when model begins to memorize training data rather than learning to generalize from trend.

The performance of the proposed methodology is compared with that of the existing approaches on the same database and the classification accuracy is shown in Table

3.3. In the literature, different approaches have been used to partition the dataset for classification. Some of the existing methods used fixed approach, in which some percentage of the data is used for training and remaining data is used for testing. However, the percentage of the data used for training and testing vary from method to method. Other existing works used leave one out method (LOOM). In the presented work, 10-fold cross validation method is used for evaluating classification performance. It can observed that proposed method outperforms the existing methods, specifically our results are better than the 1D-EMD based approach presented in [30].

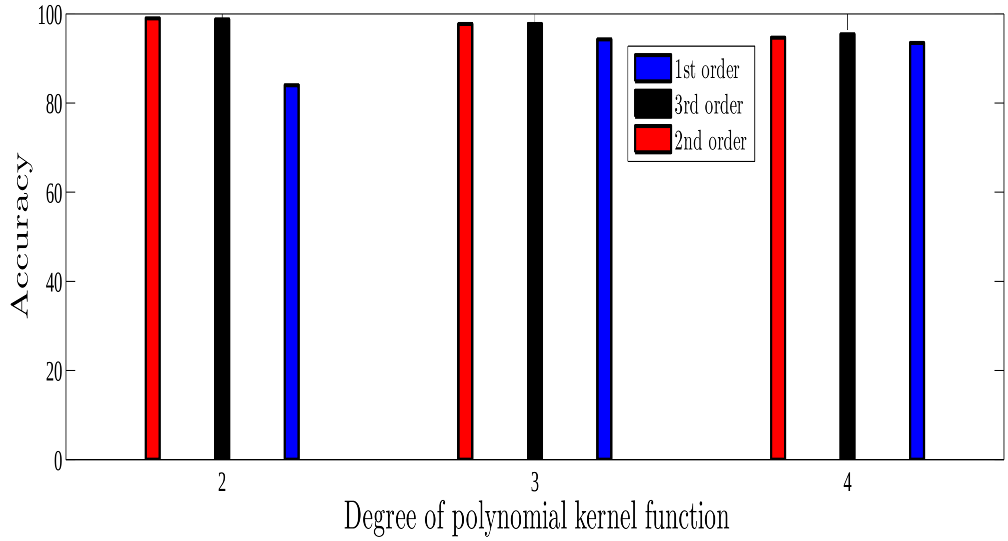

Figure 3.4: Plot of classification accuracy versus degree of polynomial kernel function in SVM.

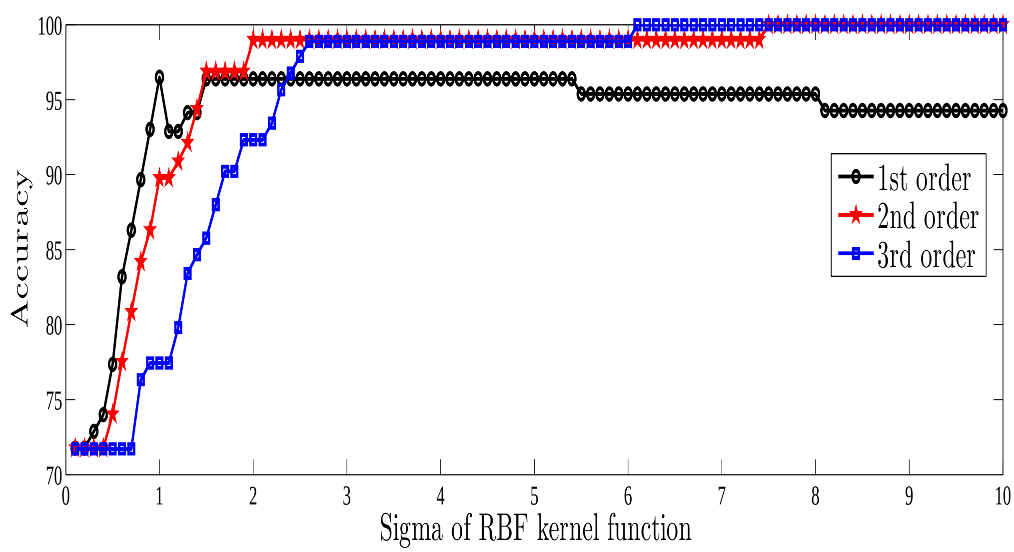

Figure 3.5: Plot of classification accuracy versus sigma of RBF kernel function in SVM.

Table 3.2: Performance of the proposed approach for classification of brain MR images

Order of AR model	kernel	Accuracy (%)	Sensitivity (%)	Specificity (%)
1^{st}	Polynomial	94.27	95.23	96.66
1^{st}	Linear	93.30	95.47	100
1^{st}	RBF	96.63	90.70	100
2^{nd}	Polynomial	99	98.57	86.67
2^{nd}	Linear	100	100	100
2^{nd}	RBF	100	100	100
3^{rd}	Polynomial	98.75	98.33	90.00
3^{rd}	Linear	97.63	96.66	100
3^{rd}	RBF	100	98.57	90

Table 3.3: Comparison of the proposed methodology with the existing methods studied on the same database

Methodology	Classification evaluation approach	Accuracy (%)
DWT and SOM [18]	Fixed partition	94
DWT and SVM [18]	Fixed partition	98
DWT, PCA and FP-ANN [23]	Fixed partition	97
DWT, PCA and k-NN [23]	Fixed partition	98
DWT, PCA and BPNN [19]	Fixed partition	100
DWT, Entropy and SVM [30]	LOOM	97
EMD, Entropy and SVM [30]	LOOM	99
Proposed work	10-fold cross validation	100

Chapter 4

Conclusions and Future Work

In this chapter, conclusions and future scope related to this research work have been provided.

4.1 Conclusions

In this work, we have proposed a new method based on the bi-dimensional empirical mode decomposition (BEMD) for automatic classification of brain MRIs. The features extracted from the autoregressive (AR) model of bi-dimensional intrinsic mode functions (IMFs) have been developed for classification of brain MRIs. The least squares support vector machine (LS-SVM) together with radial basis function (RBF) kernel function has provided maximum classification accuracy in the classification of brain MR images. In the proposed method, the kernel parameters have been selected based on the trial and error method. In future, it would be of interest to develop an automatic strategy for selecting kernel parameters and kernel function. The proposed technique for classification of brain MR images has been studied on limited database. It is necessary to study proposed method on large database before applying this methodology for clinical purpose.

4.2 Scope for future work

This methodology can be studied for multi-class classification problem, wherein images of brain affected with each disease can be considered as seperate class. Further performance of the propossed methodology can be validated on larger databases. In addition, this methodology can be studied on images of other parts of the body, for example retina, mammogram etc.

References

[1] J. Shiraishi, Q. Li, D. Appelbaum, and K. Doi, "Computer-aided diagnosis and artificial intelligence in clinical imaging," *Seminars in Nuclear Medicine*, vol. 41, no. 6, pp. 449 – 462, 2011.

[2] C.-M. Chen, Y.-H. Chou, N. Tagawa, and Y. Do, "Computer-aided detection and diagnosis in medical imaging," *Computational and Mathematical Methods in Medicine*, vol. 2013, 2013.

[3] E. P. Kumar, M. G. Sumithra, and P. S. Kumar, "Abnormality detection in brain MRI/CT using segmentation algorithm and 3D visualization," in *Fifth International Conference on Advanced Computing*, 2013, pp. 56–62.

[4] G. A. Wright, "Magnetic resonance imaging," *IEEE Signal Processing Magazine*, vol. 14, no. 1, pp. 56–66, 1997.

[5] H. Wang and A. A. Amini, "Cardiac motion and deformation recovery rrom MRI: a review," *IEEE Transactions on Medical Imaging*, vol. 31, no. 2, pp. 487–503, 2012.

[6] C. Catana, A. Drzezg, W.-D. Heiss, and B. R. Rosen, "PET/MRI for neurological applications," *Journal of Nuclear Medicine*, vol. 53, no. 12, pp. 449 – 462, 2012.

[7] A. G. Christodoulou, H. Zhang, B. Zhao, T. K. Hitchens, C. Ho, and Z. P. Liang, "High-resolution cardiovascular MRI by integrating parallel imaging with low-rank

and sparse modeling," *IEEE Transactions on Biomedical Engineering*, vol. 60, no. 11, pp. 3083–3092, 2013.

[8] M. Zhang, A. F. T. Mak, A. I. K. Chung, and K. H. Chung, "MRI investigation of musculoskeletal action of transfemoral residual limb inside a prosthetic socket," in *Proceedings of the 20th Annual International Conference of the IEEE Engineering in Medicine and Biology Society*, vol. 5, 1998, pp. 2741–2743 vol.5.

[9] E. F. Jackson, "Oncologic applications of functional MRI," in *Proceedings of the Second Joint EMBS/BMES Conference*, vol. 2, 2002, pp. 985–986.

[10] R. Caverly, "MRI fundamentals: RF aspects of magnetic resonance imaging (MRI)," *IEEE Microwave Magazine*, vol. 16, no. 6, pp. 20–33, 2015.

[11] J. Liu, M. Li, J. Wang, F. Wu, T. Liu, and Y. Pan, "A survey of MRI based brain tumor segmentation methods," *Tsinghua Science and Technology*, vol. 19, no. 6, pp. 578–595, 2014.

[12] M. Ganzetti, N. Wenderoth, and D. Mantini, "Whole brain myelin mapping using T1- and T2-weighted MR imaging data," *Frontiers in Human Neuroscience*, vol. 8, no. 671, 2014.

[13] B. Hargreaves, "Rapid gradient-echo imaging," *Journal of Magnetic Resonance Imaging*, vol. 36, no. 6, 2012.

[14] "AANLIB database of Harward medical school." [Online]. Available: http://www.med.harvard.edu/aanlib/.

[15] H. B. Nandpuru, S. S. Salankar, and V. R. Bora, "MRI brain cancer classification using support vector machine," in *IEEE Students Conference on Electrical, Electronics and Computer Science*, 2014, pp. 1–6.

[16] S. Lahmiri and M. Boukadoum, “Automatic detection of Alzheimer disease in brain magnetic resonance images using fractal features,” in *6th International IEEE/EMBS Conference on Neural Engineering (NER)*, 2013, pp. 1505–1508.

[17] P. Blonda, G. Satalino, A. Baraldi, and R. De Blasi, “Segmentation of multiple sclerosis lesions in MRI by fuzzy neural networks: FLVQ and FOSART,” in *Conference of the North American Fuzzy Information Processing Society*, 1998, pp. 39–43.

[18] S. Chaplot, L. M. Patnaik, and N. R. Jagannathan, “Classification of magnetic resonance brain images using wavelets as input to support vector machine and neural network,” *Biomedical Signal Processing and Control*, vol. 1, no. 1, pp. 86 – 92, 2006.

[19] Y. Zhang, Z. Dong, L. Wu, and S. Wang, “A hybrid method for MRI brain image classification,” *Expert Systems with Applications*, vol. 38, no. 8, pp. 10 049–10 053, 2011.

[20] S. Lahmiri and M. Boukadoum, “Hybrid discrete wavelet transform and gabor filter banks processing for features extraction from biomedical images,” *Journal of Medical Engineering*, vol. 2013, 2013.

[21] M. Maitra and A. Chatterjee, “Hybrid multiresolution Slantlet transform and fuzzy c-means clustering approach for normal pathological brain MR image segregation ,” *Medical Engineering Physics*, vol. 30, no. 5, pp. 615 – 623, 2008.

[22] K. K. Htike and O. Khalifa, “Comparison of supervised and unsupervised learning classifiers for human posture recognition,” in *International Conference on Computer and Communication Engineering*, 2010, pp. 1–6.

[23] E. A. El-Dahshan, T. Hosny, and A. B. M. Salem, “Hybrid intelligent techniques for MRI brain images classification ,” *Digital Signal Processing*, vol. 20, no. 2, pp. 433 – 441, 2010.

[24] K. Hackmack, F. Paul, M. Weygandt, C. Allefeld, and J. -D. Haynes, "Multi-scale classification of disease using structural MRI and wavelet transform ," *NeuroImage*, vol. 62, no. 1, pp. 48 – 58, 2012.

[25] H. Kalbkhani, M. G. Shayesteh, and B. Zali-Vargahan, "Robust algorithm for brain magnetic resonance image (MRI) classification based on GARCH variances series," *Biomedical Signal Processing and Control*, vol. 8, no. 6, pp. 909–919, 2013.

[26] N. Abdullah, U. K. Ngah, and S. A. Aziz, "Image classification of brain MRI using support vector machine," in *IEEE International Conference on Imaging Systems and Techniques .* IEEE, 2011, pp. 242–247.

[27] M. Maitra, and A. Chatterjee, "A slantlet transform based intelligent system for magnetic resonance brain image classification," *Biomedical Signal Processing and Control*, vol. 1, no. 4, pp. 299 – 306, 2006.

[28] M. Saritha, K. P. Joseph, and A. T. Mathew, "Classification of MRI brain images using combined wavelet entropy based spider web plots and probabilistic neural network," *Pattern Recognition Letters*, vol. 34, no. 16, pp. 2151–2156, 2013.

[29] S. Lahmiri and M. Boukadoum, "Brain MRI classification using an ensemble system and LH and HL wavelet sub-bands features," in *IEEE Third International Workshop On Computational Intelligence In Medical Imaging.* IEEE, 2011, pp. 1–7.

[30] S. Lahmiri and M. Boukadoum, "An application of the empirical mode decomposition to brain magnetic resonance images classification," in *Fourth Latin American Symposium on Circuits and Systems.* IEEE, 2013, pp. 1–4.

[31] E. A. El-Dahshan, H. M. Mohsen, K. Revett, and A.-B. Salem, "Computer-aided diagnosis of human brain tumor through MRI: A survey and a new algorithm," *Expert Systems with Applications*, vol. 41, no. 11, pp. 5526–5545, 2014.

[32] N. E. Huang, Z. Shen, S. R. Long, M. C. Wu, H. H. Shih, Q. Zheng, N. -C. Yen, C. C. Tung, and H. H. Liu, "The empirical mode decomposition and the hilbert spectrum for nonlinear and non-stationary time series analysis," in *Proceedings of the Royal Society of London A: Mathematical, Physical and Engineering Sciences*, vol. 454. The Royal Society, 1998, pp. 903–995.

[33] P. Flandrin, G. Rilling, and P. Goncalves, "Empirical mode decomposition as a filter bank," *IEEE Signal Processing Letters*, vol. 11, no. 2, pp. 112–114, Feb 2004.

[34] T. S. Kumar, V. Kanhangad, and R. B. Pachori, , "Classification of seizure and seizure-free EEG signals using multi-level local patterns," in *19th International Conference on Digital Signal Processing*, Aug 2014, pp. 646–650.

[35] R. B. Pachori, "Discrimination between ictal and seizure-free EEG signals using empirical mode decomposition," *Research Letters in Signal Processing*, vol. 2008, p. 14, 2008.

[36] R. B. Pachori, R. Sharma, and S. Patidar, "Classification of normal and epileptic seizure EEG signals based on empirical mode decomposition," in *Complex System Modelling and Control Through Intelligent Soft Computations*, ser. Studies in Fuzziness and Soft Computing, Q. Zhu and A. T. Azar, Eds. Springer International Publishing, 2015, vol. 319, pp. 367–388.

[37] R. Sharma, R. B. Pachori, and U. R. Acharya, "Application of entropy measures on intrinsic mode functions for the automated identification of focal electroencephalogram signals," *Entropy*, vol. 17, no. 2, p. 669, 2015.

[38] R. B. Pachori and S. Patidar, "Epileptic seizure classification in EEG signals using second-order difference plot of intrinsic mode functions," *Computer Methods and Programs in Biomedicine*, vol. 113, no. 2, pp. 494 – 502, 2014.

[39] R. Sharma and R. B. Pachori, "Classification of epileptic seizures in EEG signals based on phase space representation of intrinsic mode functions ," *Expert Systems with Applications*, vol. 42, no. 3, pp. 1106 – 1117, 2015.

[40] R. B. Pachori and V. Bajaj, "Analysis of normal and epileptic seizure EEG signals using empirical mode decomposition ," *Computer Methods and Programs in Biomedicine*, vol. 104, no. 3, pp. 373 – 381, 2011.

[41] A. Parey and R. B. Pachori, "Variable cosine windowing of intrinsic mode functions: Application to gear fault diagnosis," *Measurement*, vol. 45, no. 3, pp. 415 – 426, 2012.

[42] R. B. Pachori, D. Hewson, H. Snoussi, and J. Duchene, "Postural time-series analysis using empirical mode decomposition and second-order difference plots," in *IEEE International Conference on Acoustics, Speech and Signal Processing* , April 2009, pp. 537–540.

[43] H. Huang and J. Pan, "Speech pitch determination based on hilbert-huang transform," *Signal Processing*, vol. 86, no. 4, pp. 792–803, 2006.

[44] J. C. Nunes, Y. Bouaoune, E. Delechelle, O. Niang, and Ph. Bunel, "Image analysis by bidimensional empirical mode decomposition," *Image and Vision Computing*, vol. 21, no. 12, pp. 1019 – 1026, 2003.

[45] J. C. Nunes, O. Niang, Y. Bouaoune, E. Delechelle, and Ph. Bunel, "Texture analysis based on the bidimensional empirical mode decomposition with gray-level co-occurrence models," in *Proceedings of Seventh International Symposium on Signal Processing and Its Applications*, vol. 2. IEEE, 2003, pp. 633–635.

[46] L.-H. Qiao, W. Guo, W.-T. Yuan, K.-F. Niu, and L.-Z. Peng, "Texture analysis based on bidimensional empirical mode decomposition and quaternions," in *International Conference on Wavelet Analysis and Pattern Recognition*, July 2009, pp. 84–90.

[47] S. M . A. Bhuiyan, R. R. Adhami, H. S. Ranganath, and J. F Khan, "Aurora image denoising with a modified bidimensional empirical mode decomposition method," in *IEEE Southeastcon*. IEEE, 2008, pp. 527–532.

[48] J. Taghia and M. A. Doostari, "An image watermarking method based on bidimensional empirical mode decomposition," in *Congress on Image and Signal Processing*, vol. 5. IEEE, 2008, pp. 674–678.

[49] W.-K. Chen, J.-C. Lee, W.-Y. Han, C.-K. Shih, and K.-C. Chang, "Iris recognition based on bidimensional empirical mode decomposition and fractal dimension," *Information Sciences*, vol. 221, no. 0, pp. 439 – 451, 2013.

[50] M. U. Ahmed and D. P. Mandic, "Image fusion based on fast and adaptive bidimensional empirical mode decomposition," *13th Conference on Information Fusion*, pp. 1–6, 2010.

[51] J. Wan, L. Ren, and C. Zhao, "Image feature extraction based on the two-dimensional empirical mode decomposition," in *Congress on Image and Signal Processing*, vol. 1, May 2008, pp. 627–631.

[52] Z. He, Q. Wang, Y. Shen, J. Jin, and Y. Wang, "Multivariate gray model-based BEMD for hyperspectral image classification," *IEEE Transactions on Instrumentation and Measurement*, vol. 62, no. 5, pp. 889–904, May 2013.

[53] L. Ling, L. Ming, and L. YuMing, "Texture classification and segmentation based on bidimensional empirical mode decomposition and fractal dimension," in *First International Workshop on Education Technology and Computer Science*, vol. 2, March 2009, pp. 574–577.

[54] "MATLAB central file exchange," http://www.mathworks.com/matlabcentral/fileexchange/28761-bi-dimensional-emperical-mode-decomposition--bemd-/content/bemd.m.

[55] J.C. Nunes, S. Guyot, and E. Delchelle, “Texture analysis based on local analysis of the bidimensional empirical mode decomposition,” *Machine Vision and Applications*, vol. 16, no. 3, pp. 177–188, 2005.

[56] P. Soille, *Morphological image analysis: principles and applications.* Springer-Verlag New York, Inc., 2003.

[57] J. C. Carr, W. Fright, and R. K. Beatson , “Surface interpolation with radial basis functions for medical imaging,” *IEEE Transactions on Medical Imaging*, vol. 16, no. 1, pp. 96–107, Feb 1997.

[58] L. Vincent, “Morphological grayscale reconstruction in image analysis: applications and efficient algorithms,” *IEEE Transactions on Image Processing*, vol. 2, no. 2, pp. 176–201, 1993.

[59] M. A. Berezina, D. Rudoy, and P. J. Wolfe, “Autoregressive modeling of voiced speech,” *IEEE International Conference on Acoustics Speech and Signal Processing*, pp. 5042–5045, 2010.

[60] M. Nam and Y. Lee, “ 2D AR (1, 1) analysis of blurring image by empirical mode decomposition,” in *Computer Applications for Web, Human Computer Interaction, Signal and Image Processing, and Pattern Recognition.* Springer, 2012, pp. 118–125.

[61] S. R. Dubois and F. H. Glanz, “An autoregressive model approach to two-dimensional shape classification,” *IEEE Transactions on pattern Analysis and Machine Intelligence*, vol. PAMI-8, no. 1, pp. 55–66, Jan 1986.

[62] C. W. Anderson, E. A. Stolz, and S. Shamsunder, “Multivariate autoregressive models for classification of spontaneous electroencephalographic signals during mental tasks,” *IEEE Transactions on Biomedical Engineering*, vol. 45, no. 3, pp. 277–286, March 1998.

[63] B. Vuksanovic and M. Alhamdi, “AR-based method for ECG classification and patient recognition,” *International Journal of Biometrics and Bioinformatics*, vol. 7, no. 2, p. 74, 2013.

[64] K. Deguchi, “Two-dimensional auto-regressive model for analysis and sythesis of gray-level textures,” *Proc. of the 1st Int. Sym. for Science on Form*, pp. 441–449, 1986.

[65] V. Vapnik, *The nature of statistical learning theory.* Springer Science & Business Media, 2000.

[66] A. H. Khandoker, D. T. H. Lai, R. K. Begg, and M. Palaniswami, “Wavelet-based feature extraction for support vector machines for screening balance impairments in the elderly,” *IEEE Transactions on Neural Systems and Rehabilitation Engineering*, vol. 15, no. 4, pp. 587–597, Dec 2007.

[67] p. J. A. K.Suykens and J. Vandewalle , “Least squares support vector machine classifiers,” *Neural Processing Letters*, vol. 9, no. 3, 1999.

[68] V. Bajaj, and R. B. Pachori, “Classification of seizure and nonseizure EEG signals using empirical mode decomposition,” *IEEE Transactions on Information Technology in Biomedicine* , vol. 16, no. 6, pp. 1135–1142, Nov 2012.

[69] V. Joshi, R. B. Pachori, and A. Vijesh, “Classification of ictal and seizure-free EEG signals using fractional linear prediction ,” *Biomedical Signal Processing and Control*, vol. 9, no. 0, pp. 1 – 5, 2014.

[70] K. Polat, B. Akdemir, and S. Gne, “Computer aided diagnosis of ECG data on the least square support vector machine ,” *Digital Signal Processing*, vol. 18, no. 1, pp. 25 – 32, 2008.

[71] Z. Yan, X. You, J. Chen, and X. Ye, “Motion classification of EMG signals based on wavelet packet transform and LS-SVMs ensemble,” *Transactions of Tianjin University*, vol. 15, pp. 300–307, 2009.

[72] S. Das, M. Chowdhury, and M. K. Kundu, "Brain MR image classification using multiscale geometric analysis of ripplet," *Progress In Electromagnetics Research*, vol. 137, pp. 1–17, 2013.

[73] A. T. Azar, and S. El-Said, "Performance analysis of support vector machines classifiers in breast cancer mammography recognition," *Neural Computing and Applications*, vol. 24, no. 5, pp. 1163–1177, 2014.